HHS Public Access

Author manuscript

Cell Rep. Author manuscript; available in PMC 2018 June 24.

Published in final edited form as:

Cell Rep. 2018 May 08; 23(6): 1728–1741. doi:10.1016/j.celrep.2018.04.018.

Diet-Induced Growth Is Regulated via Acquired Leptin Resistance and Engages a Pomc-Somatostatin-Growth Hormone Circuit

Heiko Löhr[1], **Simon Hess**[1], **Mafalda M.A. Pereira**[2], **Philip Reinoß**[1], **Sandra Leibold**[1], **Christel Schenkel**[1], **Claudia M. Wunderlich**[2], **Peter Kloppenburg**[1,3], **Jens C. Brüning**[2,3,4], and **Matthias Hammerschmidt**[1,3,4,5,*]

[1]Institute of Zoology, University of Cologne, Cologne, Germany

[2]Department of Neuronal Control of Metabolism, Max Planck Institute for Metabolism Research, Cologne, Germany

[3]Cologne Excellence Cluster on Cellular Stress Responses in Aging-Associated Diseases, University of Cologne, Cologne, Germany

[4]Center for Molecular Medicine Cologne, University of Cologne, Cologne, Germany

SUMMARY

Anorexigenic pro-opiomelanocortin (Pomc)/alpha-melanocyte stimulating hormone (αMSH) neurons of the hypothalamic melanocortin system function as key regulators of energy homeostasis, also controlling somatic growth across different species. However, the mechanisms of melanocortin-dependent growth control still remain ill-defined. Here, we reveal a thus-far-unrecognized structural and functional connection between Pomc neurons and the somatotropic hypothalamo-pituitary axis. Excessive feeding of larval zebrafish causes leptin resistance and reduced levels of the hypothalamic satiety mediator *pomca*. In turn, this leads to reduced activation of hypophysiotropic somatostatin (Sst)-neurons that express the melanocortin receptor Mc4r, elevated growth hormone (GH) expression in the pituitary, and enhanced somatic growth. Mc4r expression and αMSH responsiveness are conserved in Sst-expressing hypothalamic neurons of mice. Thus, acquired leptin resistance and attenuation of *pomca* transcription in response to excessive caloric intake may represent an ancient mechanism to promote somatic growth when food resources are plentiful.

*Correspondence: mhammers@uni-koeln.de.

[5]Lead Contact

SUPPLEMENTAL INFORMATION

Supplemental Information includes Supplemental Experimental Procedures, four figures, and six tables and can be found with this article online at https://doi.org/10.1016/j.celrep.2018.04.018.

AUTHOR CONTRIBUTIONS

H.L., S.L., C.S., and P.R. conceived, designed, performed, and analyzed the zebrafish experiments. M.M.A.P. designed and performed the mouse RNA scope experiments. S.H. carried out the electrophysiology studies. C.M.W. generated the R26-fl-rxΔ-ZsGreen mouse line. H.L., P.K., J.C.B., and M.H. conceived the project, designed the study, analyzed and interpreted data, and wrote the manuscript with input from all authors.

DECLARATION OF INTERESTS

The authors declare no competing interests.

Graphical abstract

In Brief: The melanocortin system controls energy homeostasis and somatic growth, but the underlying mechanisms are elusive. Löhr et al. identify a functional neural circuit in which Pomc neurons stimulate hypothalamic somatostatin neurons, thereby inhibiting hypophyseal growth hormone production. Excessive feeding and acquired leptin resistance attenuate this pathway, allowing faster somatic growth when food resources are rich.

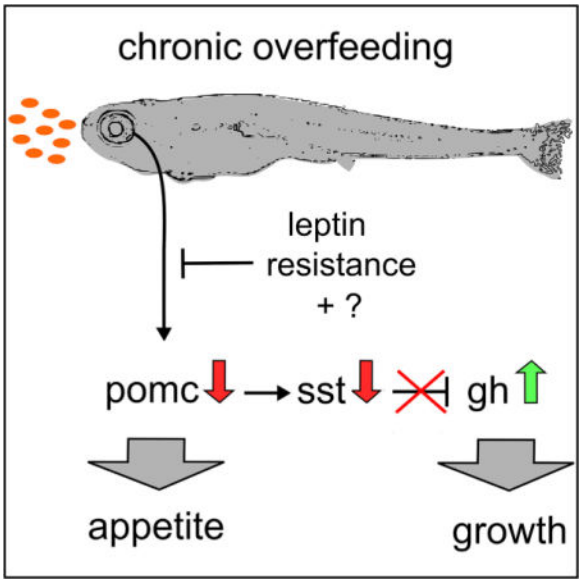

INTRODUCTION

Excessive energy intake is associated with obesity and increased linear growth, suggesting a coordinated interplay between systems controlling energy homeostasis and the somatotropic axis (He and Karlberg, 2001; Savastano et al., 2014). A key neuroendocrine network involved in regulating food intake and metabolism in vertebrates is the melanocortin (MC) circuitry of the hypothalamus (Krashes et al., 2016; Timper and Brüning, 2017). Here, two antagonistic neuronal populations of the arcuate nucleus, releasing either Agouti-related peptide (Agrp) or the Pomc-derived peptide alpha-melanocyte stimulating hormone (αMSH), sense the energy state of the organism via hormonal and nutritional signals from the periphery, including leptin, or are regulated by centrally derived signals (Chen et al., 2015; Garfield et al., 2016). αMSH binds and activates melanocortin 4 receptor (Mc4r) expressed on distinct second-order neurons and conveys anorexigenic responses (decreased food uptake and increased energy expenditure), whereas the orexigenic peptide Agrp functions as an antagonist or inverse agonist of Mc4r. Pomc and Agrp neurons form extensive projections throughout the brain, including main target areas involved in energy homeostasis control, such as the paraventricular nucleus (PVN) of the hypothalamus (King and Hentges, 2011; Wang et al., 2015). In mammals, genetic loss of leptin (Zhang et al., 1994), Pomc (Yaswen et al., 1999), or Mc4r (Huszar et al., 1997) function leads to severe obesity (Krashes et al., 2016; Timper and Brüning, 2017). Diet-induced obesity in genetically unaffected individuals can be enhanced by a phenomenon called acquired leptin

resistance, with reduced leptin receptor signal transduction in, and reduced activation of, Pomc cells despite high leptin serum levels. While the exact molecular mechanisms underlying this phenomenon are elusive, they appear to involve an overactivation of cell-autonomous negative feedback responses (Enriori et al., 2007; Friedman, 2014, 2016; O'Rahilly, 2014).

In addition to obesity, loss-of-function mutations in Pomc or Mc4r also result in moderately enhanced linear growth both in rodents (Huszar et al., 1997; Yaswen et al., 1999) and humans (Farooqi et al., 2000; Krude et al., 2003; Martinelli et al., 2011). Somatic growth is primarily regulated via growth hormone (GH) released by somatotrophes in the adenohypophysis of the pituitary gland. GH expression and release by somatotrophes is inhibited by Sst-expressing neurons of the periventricular nucleus (PeVN) and PVN, while hypothalamic GH-releasing hormone (Ghrh)-expressing neurons have opposite effects on GH (Tauber and Rochiccioli, 1996; Eigler and Ben-Shlomo, 2014). However, the molecular basis of melanocortin-dependent control of somatic growth remains enigmatic, and neither Sst nor Ghrh cells had been identified as second-order neurons of the melanocortin system as yet.

In zebrafish, the somatotropic and melanocortin systems are remarkably conserved. Similar to mammals, zebrafish GH (*gh1*)-expressing cells are located in the zebrafish adenohypophysis, and *gh1* mutants display strongly decreased somatic growth (McMenamin et al., 2013), whereas the neuroanatomy and function of Sst and Ghrh neurons in the context of somatic growth have not been studied in this species. Moreover, zebrafish Pomca and Agrp neurons are located in hypothalamic domains homologous to the mammalian arcuate nucleus (Forlano and Cone, 2007), and studies in different teleost species suggest a conserved function of the melanocortin system in control of energy homeostasis (Cerdá-Reverter et al., 2011). In addition, the zebrafish melanocortin system affects somatic growth; transgenic overexpression of Agrp results in increased *gh1* expression and body length (Song and Cone, 2007), whereas morpholino-based *agrp* knockdown has opposite effects (Zhang et al., 2012). These effects were assigned to a direct innervation of the adenohypophysis by Pomc and Agrp neurons (Zhang et al., 2012) rather than involving Sst neurons as mediators.

Here, we provide first evidence for the existence and functionality of such a Pomc-Sst-Gh axis in zebrafish and mouse regulating somatic growth dependent of caloric energy availability.

RESULTS

Long-Term Caloric Excess Increases Growth Rate and Lipid Metabolism of Larval Zebrafish

In order to analyze the interplay between energy supply and linear growth during zebrafish development, we applied different feeding conditions to zebrafish larvae starting at 5 days post-fertilization (dpf): (1) low-density suspension of live paramecia representing limited food resources (LD), (2) high-density paramecia suspension representing *ad libitum* feeding conditions (HD), and (3) HD paramecia plus additional daily supply of egg yolk

representing *ad libitum*/high-fat diet conditions (HD/HF). Such differences in feeding regimes affected not only linear/somatic growth but also the developmental pace of larvae, as judged by anatomical staging (Parichy et al., 2009) (Figures S1A–S1C and S1N–S1V) and similar to what has been shown in juvenile fish (Leibold and Hammerschmidt, 2015). Therefore, comparative analyses were performed not only between age-matched larvae (15 dpf) of different sizes (Figures S1A–S1M) but also primarily between size-matched larvae of a standard length of 6 mm (Figures 1A–1D), which was obtained at 13 dpf for HD/HF, 14 dpf for HD, and 18 dpf for LD larvae, respectively. Examination of visceral neutral lipid droplets by Nile red staining revealed larger lipid depots in the HD and HD/HF groups than in the LD group (Figure 1E). Consistently, HD and HD/HF larvae displayed moderately increased expression of fatty acid binding protein 11a (*fabp11a*), a marker for differentiated adipocytes (Imrie and Sadler, 2010), and of the adipokine adiponectin b (*adipoqb*), and strongly increased expression of the two leptin paralogs *lepa* and *lepb*. In contrast, expression of peroxisome proliferator-activated receptor gamma (*pparg*), marking both developing and mature adipocytes (Gesta et al., 2007), was unaltered (Figure 1F). Since obesity is commonly associated with hyperinsulinemia, we also analyzed insulin (*insa*) expression and found increased *insa* expression in the HD group, but not in the HD/HF group, compared to the LD control (Figure 1F). Together, this indicates that long-term high fat-diet promoted both somatic growth and obesity, but not necessarily hyperinsulinemia.

Long-Term Caloric Excess Causes Leptin Resistance and Affects Both the Melanocortin and GH System

We also assessed transcript levels of *gh1* and the two melanocortin peptides *pomca* and *agrp* (Figure 2A). *gh1* levels were significantly elevated in the HD and HD/HF groups compared to the LD group. In contrast, *agrp* levels were similar in all groups, whereas *pomca* levels were significantly decreased in the HD and HD/HF groups compared to the LD group. *pomca* is expressed in the hypothalamus and the adenohypophysis (Forlano and Cone, 2007) and HD/HF-induced *pomca* reduction was even stronger in larvae from which the pituitary had been manually removed, revealing that it primarily reflects changes in hypothalamic *pomca* expression. Consistently, the expression of markers of defined second-order neurons downstream of Pomca and Agrp neurons was also reduced after excessive feeding (Figure 2A), such as thyroptropin-releasing hormone (*trh*) and oxytocin (*oxt*) (Kim et al., 2000; Sabatier et al., 2003). In contrast, studies in *pomca:EGFPras* transgenic reporter fish (see below for more details) revealed that HD and HD/HF feeding did not affect the number of Pomca neurons (Figure 2B), pointing to a specific effect on *pomca* transcription. Similar results were obtained when comparing age-matched LD, HD, and HD/HF larvae at 15 dpf (Figures S1D–S1M). At first sight, this negative regulation of *pomca* expression by food intake is a surprising finding for a satiety-signaling neuropeptide. However, this effect was only observed upon long-term overfeeding. In contrast, larvae exposed to a high-fat diet for only 6 hr displayed unaltered *gh1* and *agrp* expression levels but significantly increased *pomca* transcription (Figure 2C), in line with the response of *Pomc* to acute overfeeding in mammals.

Next, we aimed to investigate the mechanism underlying reduction of *pomca* transcription upon prolonged overfeeding. In mammals, transcription from the *Pomc* promoter is

controlled by leptin and insulin signal transduction pathways (Varela and Horvath, 2012), while diet-induced obesity has been shown to cause severe but reversible leptin resistance of Pomc cells, characterized by low Pomc cell activation despite high leptin production by adipocytes (Enriori et al., 2007). Consistently, we found that in contrast to their LD controls, Pomca neurons of HD/HF zebrafish larvae failed to be activated upon treatment with human leptin as determined via phosphorylated version of extracellular signal-regulated kinase (pERK) immunofluorescence (IF) in the *pomca:EGFPras* transgenic line (Figures 2D–2I) (see below). In addition, juvenile zebrafish subjected to excessive feeding for 10 days displayed a much weaker induction (1.1-fold increase) of *pomca* transcription after intracerebroventricular (ICV) injection of human leptin than their respective normally fed controls (1.7-fold increase; Figure 2J).

Together, this indicates that reduced *pomca* expression in conjunction with elevated *gh1* expression is a specific consequence of long-term *ad libitum*/high-fat diet feeding, which is at least partly mediated by the evolutionary conserved occurrence of acquired leptin resistance.

Pomca Cells Do Not Project into the Adenohypophysis, and Pomca Innervation of the POA Is Not Altered upon Long-Term Overfeeding

In order to directly study Pomca neurons and their circuits in the context of somatic growth, we generated *pomca:EGFPras* (see also above) and *pomca:KaITA4* (attenuated Gal4VP16) transgenic zebrafish lines, which both fully recapitulate endogenous *pomca* expression (Figures S2A and S2B; data not shown). Pomca cell fibers built a complex network (Figure 3A), including innervations of the preoptic area (POA), the functional homolog of the rodent PVN (Herget et al., 2014; Peter, 1977), to where they send projections in very near proximity to *oxt*-, *trh*-, and *crh*-expressing cells (Figures 3E–3G). Notably, previous studies in zebrafish reported intense innervation of the pituitary by αMSH-positive axons (Zhang et al., 2012). However, in the *pomca:EGFPras* transgenic larvae, we only found few projections toward the pituitary. Most Pomca axons ran dorsal of the pituitary to cross the midline (Figures 3B–3D), or lateral of it (Figures 3C and 3D), and few axons entered the neurohypophysis (Figure 3C), while not a single projection was observed to directly target the adenohypophysis (Figures 3B–3D and S2C). Consistently, retrograde labeling of pituitary projections in *pomca:EGFPras* juveniles at 42 dpf failed to label hypothalamic Pomca neurons (Figure S2D), while IF analyses suggest that the former detection of hypophyseal axonal αMSH might have been caused by a cross-reactivity of the αMSH antibody with melanin-concentrating hormone (MCH) (Figures S2E–S2G).

In rodents, overnutrition during a critical time period of melanocortin system development is characterized by reduced Pomc cell projections to hypothalamic targets (Vogt et al., 2014). Instead, analysis of the Pomca cell circuitry in *pomca:EGFPras* transgenic zebrafish subjected to the long-term feeding paradigm revealed no detectable changes in POA innervation among the LD, HD, and HD/HF groups as assessed by quantification of axons innervating the POA or crossing the anterior commissure (Figures 3H–3L). Thus, distinct to rodents, overfeeding and/or application of a high-fat diet to zebrafish during stages of Pomca

circuit development does not impair establishment of POA innervation. This may allow fish (in contrast to mammals) to better adapt to changes in environmental food availability.

Pomca Neurons Inhibit GH Expression

To investigate the function of Pomca neurons in the context of somatic growth, we used the nitroreductase (*nfsb*)/metronidazole (MTZ) system (Curado et al., 2008) to ablate hypothalamic and hypophyseal Pomca cells during late larval stages by treating *pomca:KalTA4*;*UAS:nfsb-Cherry* double transgenic fish with MTZ (Figures 4A and 4B). Pomca cell ablation resulted in a strong reduction of *pomca* transcript levels but a significant increase in *gh1* levels relative to non-ablated controls (Figure 4C). This effect can be fully attributed to the hypothalamic fraction of the Pomca cell population, as pituitary-specific ablation of Pomca cells with the *pomca*(pit):*CFP-nfsb* transgene still resulted in a reduction of *pomca* levels, whereas *gh1* expression levels remained unaffected (Figures 4D–4F). This negative effect of hypothalamic Pomca cells on *gh1* expression was further confirmed by pharmacological treatment of zebrafish larvae: incubation for 24 hr in medium containing 10 μM αMSH resulted in a significant reduction of *gh1* expression, whereas opposite effects were observed upon treatment with 10 μM of the Mc4r antagonist SHU9119 (Figure 4G). Collectively, this indicates that Pomca neurons inhibit *gh1* expression in an αMSH-dependent manner.

Pomca Cells Are Anatomically Connected to the Hypothalamo-Hypophyseal Somatotropic Axis

Neuroanatomical analyses in the *pomca:EGFPras* transgenics presented above clearly indicated that Pomca neurons do not directly project to the adenohypophysis but instead favor the possibility that second-order neurons are involved in mediating their negative effect on *gh1* expression and function. Sstexpressing hypothalamic neurons, well-characterized components of the somatotropic hypothalamo-hypophyseal axis, appeared as likely candidates, although so far have not been linked to the melanocortin circuitry, even in mammals. The zebrafish genome contains five different somatostatin genes, with *sst1.1* showing various expression domains, including the POA (Löhr et al., 2009). To analyze the projection patterns of zebrafish Sst1.1 neurons, we generated an *sst1.1:EGFPras* transgenic line (Figure 5A) that fully re-capitulates the endogenous sst1.1 expression (Figures S3A and S3B) and defines an anterior and posterior Sst1.1 cell domain within the POA (Figure 5D′). Strikingly, in contrast to Pomca cell projections (see above), the *gh1* domain of the larval adenohypophysis was intensely labeled by Sst1.1+ projections (Figure 5B). Retrograde labeling with DiI crystals placed into the pituitary of *sst1.1:EGFPras* juveniles (30 dpf) identified cells of the posterior POA cluster as the Sst1.1 neurons directly projecting to the adenohypophysis, whereas cells in the anterior POA domain or any other brain region did not reveal any co-label (Figures 5C–5D′; data not shown; n = 7/7).

In order to test whether such hypophysiotropic Sst1.1 cells can serve as direct targets for Pomca neurons and αMSH, we carried out *sst1.1 in situ* hybridization (ISH) and anti-GFP IF on *pomca:EGFPras* transgenics, revealing a clear pattern of innervation of the posterior Sst1.1 domain by Pomca cell axons (Figures 5E–5G) at all examined developmental stages. In addition, co-labeling *sst1.1:EGFPras* larvae via *mc4r* ISH and anti-GFP IF revealed broad

expression of *mc4r* within the POA (Figures 6A–6A″), including hypophysiotropic Sst1.1+ cells of the posterior POA domain (Figures 6B–6B″). Together, this points to the presence of all neuroanatomical and structural prerequisites for a functional Pomca-Sst1.1-Gh1 hypothalamo-hypophyseal axis in the zebrafish brain. Strikingly, also in the mouse, 58.4% ± 10.2% of hypophysiotropic Sst cells of the PeVN/PVN (Figures 6C and 6C′) displayed Mc4r expression (Figures 6D–6F). In reverse, 10.3% ± 4.1% of Mc4r+ cells of the mouse PeVN/PVN displayed Sst expression, consistent with the formerly reported co-existence of Sst cells with multiple other potential αMSH target cells in this area (Biag et al., 2012) and similar to the incomplete overlap of *sst1.1* and *mc4r* expression in the zebrafish POA (Figures 6A–6B″). Together, this points to the evolutionary conservation of Pomc-Sst circuitry.

Functional Connection between αMSH, Sst1.1 Neurons and Somatostatin

We next set out to assess the functional impact of αMSH on hypophysiotropic Sst cells in fish and mouse. Perforated patch clamp recordings were performed in *Sst-IRES-Cre*;*R26-fl-rx*Δ-*ZsGreen* double transgenic mice (Experimental Procedures) from Sst PeVN neurons, which were pharmacologically isolated from GABAergic and glutamatergic input to minimize indirect modulatory effects. The neurons were identified by their position in the PeVN and by their fluorescent label (Figure 6G). 250 nM αMSH was bath-applied for 5–7 min, and the effect was measured 10 min after the onset of αMSH administration. In average, αMSH increased action potential frequency by ~43% (from 3.0 ± 1.1 Hz to 4.3 ± 1.3 Hz; $p = 0.009$, $n = 6$). On the single-cell level, a significant increase in action potential frequency was observed in two-thirds of the recorded Sst neurons (Figure 6I), consistent with the obtained percentage of Sst neurons displaying Mc4r expression (Figure 6F). Of note, typically the stimulatory effect of αMSH continued to increase even further throughout the first ~15 min of the washout and was not fully reverted even after a >30-min wash (Figure 6H), in line with the previously reported effects of αMSH on Mc4r+ PVN neurons (Ghamari-Langroudi et al., 2011).

To investigate the effect of αMSH on zebrafish Sst cells, we isolated the brains of *sst1.1:EGFPras* juveniles (42 dpf) and incubated one brain hemisphere in artificial cerebrospinal fluid (ACSF) and the other hemisphere in ACSF containing 10 μM αMSH. After incubation for 30 min, the αMSH-treated hemisphere displayed a strong increase of pERK levels, indicative of neuronal activation (Randlett et al., 2015), in hypophysiotropic Sst1.1 neurons of the posterior POA domain compared to the control hemisphere (Figures 7A–7G). Similar results were obtained upon ICV injection of 0.5 mg/kg αMSH into juvenile *sst1.1:EGFPras* fish at 42 dpf compared to saline-injected controls (Figures S2C and S2D). Furthermore, repetitive ICV injections of saline, 0.5 mg/kg αMSH, or 0.5 mg/kg SHU9119 over the course of 48 hr (saline: $n = 17$; αMSH: $n = 11$; SHU9119: $n = 15$) slightly increased or decreased *sst1.1* fluorescent ISH signal within the posterior POA domain 2 hr after the last αMSH or SHU9119 injection, respectively (Figure 7H). Finally, to test whether the effect of αMSH on somatic growth depends on somatostatin function, we carried out a pharmacogenetic epistasis analysis (Figure 7I). For this purpose, we treated zebrafish larvae at 14 dpf for 8 hr with 10 μM αMSH, 1 μM of the nonselective somatostatin receptor antagonist cyclo-somatostatin (cSST), or a combination of both and determined the effects

on *gh1* transcript levels. αMSH treatment significantly reduced *gh1* expression compared to saline-treated controls, as reported above, while this effect was fully abrogated upon co-treatment with cSST.

Together, this indicates that the negative effect of αMSH on *gh1* transcription and somatic growth is mediated via somatostatin released by Sst1.1 neurons, which are direct targets of Pomca neurons and therefore hereby newly identified second-order neurons of the melanocortin system.

DISCUSSION

In the present study, we investigated the relationship between the melanocortin and somatotropic systems in zebrafish, an organism that displays a strong diet dependence of somatic growth (Leibold and Hammerschmidt, 2015). We identify a thus-far-unknown hypothalamo-hypophyseal αMSH/Pomcasomatostatin-GH axis promoting growth upon excessive food supply. Somatostatin-producing Sst1.1 neurons of the hypothalamic POA are a central part of this axis. These Sst1.1 cells are innervated by Pomca neurons, express the αMSH receptor Mc4r, and can be stimulated by exogenous αMSH. Thus, they fulfill all criteria to be regarded as second-order neurons of the melanocortin system, while in turn projecting to the pituitary to attenuate *gh1* expression. In accordance with such a net growth-inhibiting effect of Pomca/αMSH, ablation of Pomca neurons or treatment with an Mc4r antagonist led to increased, and treatment with αMSH to decreased *gh1* transcript levels. Strikingly, in co-treatment experiments, αMSH failed to attenuate *gh1* expression when endogenous somatostatin was inhibited, clearly indicating that its negative impact on growth is indirect and mediated in an Sst-dependent manner. These functional features are consistent with the structural equivalents of this circuitry as revealed through our transgenic reporter lines. In contrast, in a former report, the effect of the melanocortin system on *gh1* production had been attributed to direct αMSH and Agrp neuronal projections to the pituitary (Zhang et al., 2012), a mechanism that, according to our data, is of minor importance. However, the overall growth-promoting effect of Agrp reported by Zhang et al. (2012) is consistent with the growth-inhibiting effect of αMSH and Pomca neurons reported here.

A fundamental question remains: why do αMSH/Pomca neurons inhibit growth, given that they are normally active after feeding and when energy stores are filled, activated by energy-sensing signals like leptin to reduce appetite and promote energy expenditure? We recently showed that in zebrafish, somatic growth can be subordinate to other anabolic branches of energy expenditure, such as developmental pace in larvae and reproduction in adults (Leibold and Hammerschmidt, 2015). In this light, it makes sense in the short-term to attenuate *gh1* levels to reserve energy for biological processes other than growth and/or to reduce *gh1*-dependent lipolysis (McMenamin et al., 2013), thereby protecting lipid energy stores. In addition, such negative short-term effects might contribute to the circadian variations in GH secretion, which during wakeness (when food is taken up) is much lower than during sleep (Van Cauter et al., 1998).

Interestingly and most strikingly, however, we also found that this per se growth-inhibiting pathway can also be used to promote growth, when under conditions of long-term *ad libitum* feeding, *pomca* transcript levels do not rise, as only seen in short-term response to overfeeding, but even decline. This in turn results in decreased Sst1 neuron activation and a de-repression of *gh1* expression. Thereby, it is ensured that upon continuously rich food resources, when energy prioritization is no longer required, larval zebrafish switch into a "seize-the-opportunity" mode, with reduced *pomca* levels allowing for unrestricted food intake and somatic growth. We could further show that this reduction in *pomca* transcription correlates with and might be caused by diet-induced leptin resistance of hypothalamic Pomca cells, similar to what has been reported for mammals (Enriori et al., 2007). However, leptin resistance was only demonstrated for exogenously supplied leptin, raising the possibility that our *ad libitum* fed fish are still capable of responding to endogenous leptin, similarly to what has been reported for diet-induced obese mice (Ottaway et al., 2015; Myers, 2015). Also, acquired leptin resistance per se can explain why *pomca* transcript levels in *ad-libitum*-fed fish are not higher, but not necessarily why they are even lower than in controls with restricted food supply. Therefore, it seems likely that other dietary factors in addition to diet-induced leptin resistance target the melanocortin system to regulate the activity of the somatotropic axis. However, all of these factors and mechanisms seem to interfere with the melanocortin system at the hormonal, rather than the anatomical level, as Pomca cell circuits' architecture remained unaltered in *ad-libitum*-fed fish. This is in contrast to findings in mouse where feeding high caloric diets to mothers during the lactation period impairs projections of both of POMC and Agrp neurons to various hypothalamic target nuclei (Vogt et al., 2014).

We have also obtained the first data suggesting that a Pomc-Sst-Gh axis is also active in mammals. GH transcription and release have long been known to be under negative control of Sst and positive control of Ghrh (Tauber and Rochiccioli, 1996). There was also indirect support for a functional correlation between Pomc and Sst, with obese/large Agouti-yellow mice displaying increased levels of the αMSH antagonist Agouti in combination with decreased Sst levels in the PeVN, whereas Ghrh levels are unaltered (Martin et al., 2006). However, whether mouse Sst neurons of the PeVN express Mc4R and respond to αMSH had not been elucidated before and is now shown here. Clearly, in contrast to fish, excessive food intake in mammals primarily promotes fat storage and obesity development, yet obese mammals also display a moderate increase in linear body size (Krude et al., 2003; Lu et al., 1994; Martinelli et al., 2011). Together, this suggests that a Pomc-Sst-Gh axis might also exist in mammals but might be less pronounced than in zebrafish or other teleosts with an even more advanced indeterminate growth. In addition, it appears that in conjunction with a strong Pomc-Sst-Gh axis, as in fish, diet-induced leptin resistance, possibly in cooperation with other diet-induced mechanisms, can elicit a favorable and possibly original function to promote unrestricted growth when food resources are rich, whereas in conjunction with a weaker axis, as in mammals, its adverse effects dominate, worsening obesity by attenuating the main negative feedback mechanism to burn energy and to restrict food uptake. Thus, leptin resistance may represent an evolutionary conserved concept that originated to sense long-term availability of rich fuel sources to allocate energy to somatic growth.

EXPERIMENTAL PROCEDURES

Zebrafish Lines and Mice Strains

The *Tg(pomca:EGFPras)*^{fr38Tg}, *Tg(pomca:KaITA4)*^{fr39Tg}, *Tg(sst1.1:EGFPras)*^{fr40Tg}, and *Tg(pomca(pit):CFP-nfsb;cmlc2:GFP)*^{fr41Tg} zebrafish lines were generated during the course of this study (Supplemental Experimental Procedures). The *Tg(UAS-E1b:nfsb-mCherry)*^{c264} line was previously described (Davison et al., 2007). All zebrafish experiments were approved by the national animal welfare committees (LANUV Nordrhein-Westfalen; 8.87–50.10.31.08.129; 84–02.04.2012.A251; 84–02.04.2012.A390; City of Cologne; 576.1.36.6.3.01.10 Be) and the University of Cologne. C57BL/6 mice were purchased from Charles River Laboratories, *Sst-IRES-Cre* mice (Taniguchi et al., 2011) from The Jackson laboratory (stock number 013044). For generation of *R26-fl-rx*Δ*-ZsGreen* transgenic and *Sst-IRES-Cre; R26-fl-rx*Δ*-ZsGreen* double transgenic mice, see Supplemental Experimental Procedures. Mice were housed under controlled environment in a 12h light/dark cycle, with food and water *ad libitum*. The procedures were approved by the Bezirksregierung (local authority in Cologne, Germany).

Larval Feeding Experiments

Starting at 5 dpf, 30 larvae per feeding group were transferred to plastic cylinders with a meshed bottom (9 cm diameter), each placed in a 1l beaker and filled with 200 mL of the appropriate paramecia suspension. Different concentrations of paramecia were obtained by directly feeding the stock culture (condition: high density [HD]), which corresponds to 400–500 paramecia per milliliter, or further diluting the stock 1:2 (condition: low density [LD]) in embryo medium. To generate high-caloric feeding conditions (HD/HF), larvae fed with concentrated paramecia stock were removed once per day from the cylinders and transferred to 50-mL tubes containing 30–40 mL 10% egg yolk (Proteinvital/Austria; 34% protein, 56% fat, and 4% carbohydrates) in embryo medium. Egg-yolk-treated larvae were incubated on a horizontal shaker for 6 hr and then returned to cylinders. Paramecia suspensions of all groups were exchanged once per day after egg yolk incubations. For acute egg yolk treatment, LD group larvae were incubated in 10% egg yolk for 6 hr at 14 dpf before sample collection.

Pharmacological Treatments

For pharmacological treatments of live zebrafish larvae, 6–8 specimen (14 dpf) per condition were incubated in 5 mL buffered embryo medium in a 6-well plate. Concentrations used were 10 μM αMSH (Sigma-Aldrich), 10 μM SHU9119 (Phoenix Pharmaceuticals), or 1 μM cSST (Tocris Bioscience). For controls, embryo medium without chemical additive was used. Incubation was performed in the dark at 28°C. αMSH and SHU9119 were applied for 24 hr. For the epistasis study (Figure 7I), αMSH, cSST, or a combination of both was applied for 8 hr. During chemical treatments, larvae did not receive food. After treatments, larvae were stored in Trizol until further processing.

For treatment with recombined human leptin (Figures 2D–2I), *pomca:EGFPras* transgenic larvae raised under LD or HD/HF conditions were sacrificed, the head was cut off, and the skull was opened/removed dorsally with fine forceps to allow diffusion of leptin into brain

tissue. Heads were then incubated in ACSF (134 mM NaCl, 2.9 mM KCl, 2.1 mM $CaCl_2$, 1.2 mM $MgCl_2$, 10 mM glucose, and 10 mM HEPES, 290 mOsm, pH 7.8) with or without leptin (10 μM; Phoenix Pharmaceuticals) for 30 min at room temperature and fixed in 4% paraformaldehyde/PBS containing 0.25% TritonX.

For treatments of hemisphere explants (Figures 7A–7G), *Tg(sst1.1:EGFPras)*^{fr40Tg} juvenile fish (42 dpf) were sacrificed, brains were removed from the skull, and the two brain hemispheres were separated with a blade. For each brain, one hemispherewasincubatedin1mLACSF, andtheotherhemispherewasincubated in ACSF supplemented with 10 μM αMSH. After a 30-min incubation at room temperature, hemispheres were fixed in 4% paraformaldehyde/PBS containing 0.25% TritonX.

Cell Ablations

For global Pomca cell ablation, 15 double transgenic larvae (mCherry+) and 15 control siblings (mCherry−) from a cross of a *Tg(pomca:KalTA4)*^{fr39Tg} and a *Tg(UAS-E1b:nfsb-mCherry)*^{c264} transgenic fish were pre-sorted and collectively raised in one container to ensure identical feeding and raising conditions for both genotypes. For pituitary-specific Pomca cell expression, 15 transgenic larvae and 15 control siblings derived from a Tg(*pomca(pit):CFP-nfsb;cmlc2:GFP*)^{fr41Tg} outcross to a wild-type fish were raised in one container. Starting at 12 dpf, the larvae were treated with 7 mM Mtz (Sigma-Aldrich) for 48 hr followed by withdrawal of Mtz and a 18- to 20-hr recovery period. During treatment and recovery, larvae were supplied with food. The paramecia/Mtz suspension was exchanged once after 24-hr treatment. After ablation, *Tg(pomca:KalTA4)*^{fr39Tg}, *Tg(UAS-E1b:nfsb-mCherry)*^{c264} double transgenic larvae displayed well-visible remnants of mCherry signal in the pituitary and were separated from the controls at a fluorescent stereomicroscope. For *Tg(pomca(pit):CFP-nfsb;cmlc2:GFP)*^{fr41Tg} samples, the *cmlc2:GFP* reporter was used to separate transgenic from control larvae. All samples were stored in Trizol (Thermo Fisher Scientific) until used for further processing.

DiI Injections

Crystals of lipophilic carbocyanine dye (DiI; Thermo Fisher Scientific) were placed in the pituitary of *Tg(sst1.1:EGFPras)*^{fr40Tg} or *Tg(pomca:EGFPras)*^{fr38Tg} juvenile fish (30–42 dpf) using a microinjection setup. Briefly, fish were euthanized with tricaine and decapitated, and ventral head tissue was removed to expose the pituitary. After injection, the head was placed in 4% paraformaldehyde, and DiI was allowed to diffuse for 1 week at 4°C. After incubation, the brains were removed from the skull, washed with PBS, and directly imaged using a confocal microscope.

ICV Microinjections

Cerebroventricular microinjections were performed as previously described (Kizil and Brand, 2011). *Tg(sst1.1:EGFPras)*^{fr40Tg} juvenile fish (42 dpf) received 0.5 μg/g bodyweight αMSH or SHU9119 (injection volume, 500 nl) diluted in fish ACSF. Controls received ACSF only. For analysis of pERK activation (Figures S2C and S2D), fish received one injection of αMSH and were sacrificed 30 min post-injection, followed by fixation in 4% paraformaldehyde/PBS containing 0.25% TritonX. For evaluations of the long-term effects

of αMSH and SHU9119 (Figure 7H), injections were performed twice a day during a 48-hr course. After each injection round, fish were connected to water circulation and food was supplied. 2 hr after the last injection, fish were sacrificed and brains were fixed in 4% paraformaldehyde/PBST (phosphate-buffered saline supplemented with 0.1% Tween 20). For leptin injections, wild-type juvenile fish were normally fed or excessively overfed (using carbohydrate- and lipid-rich dry food) from 42 to 51 dpf, followed by a single ICV injection of 1.0 μg/g bodyweight human leptin (Phoenix Pharmaceuticals) diluted in ACSF. Controls received ACSF only. Fish were euthanized 4 hr post-injection, and brains were removed and stored in Trizol (Figure 2J).

qRT-PCR

RNA from all samples was isolated using Trizol Reagent (Thermo Fisher Scientific) with the PureLink RNA Mini Kit (Thermo Fisher Scientific) including on-column DNaseI treatment followed by reverse transcription with Superscript II reverse transcriptase (Thermo Fisher Scientific). Gene expression was assayed by qPCR with SYBR Select Master Mix (Thermo Fisher Scientific) for *pparg*, *fabp11a*, *adipoqb*, *gh1, crh*, *trh*, *oxt*, *insa*, and normalized against ribosomal protein S23 transcript (*rps23*) (see Table S4 for primer sequences), or with TaqMan assays (Thermo Fisher Scientific) for *agrp*, *lepa*, *lepb*, and *pomca* also normalized against *rps23* (see Table S5 for assay IDs). qPCR was performed on an ABI-PRISM 7500 Fast Detection system. Fold differences were calculated using the $\Delta\Delta C_T$ method. For quantification of hypothalamus-specific *pomca* expression, the pituitary was removed from larvae using the *tg(pomca:EGFPras)*^{fr40Tg} line to control for complete removal.

Tissue-Labeling Procedures

Whole-mount fluorescent ISH (FISH), and whole-mount IF staining of zebrafish larvae were carried out as described in Supplemental Experimental Procedures. For Nile red staining of neural lipids, zebrafish larvae were incubated in a solution of 0.5 μg/ml Nile red (Sigma-Aldrich) for 10–15 min, carefully washed, and immediately subjected to imaging.

Detection of *Mc4r* and *Sst1* transcripts on mouse brain sections was carried out via RNAscope as described in the Supplemental Experimental Procedures.

Electrophysiology

Perforated patch-clamp experiments were performed on coronal brain slices (250–300 μm) from female and male $Sst^{ZsGreen}$ mice (6–9 weeks of age), which contained the PeVN. Experiments were carried out essentially as described previously (Hess et al., 2013; see Supplemental Experimental Procedures for details).

Statistics

All experiments were independently repeated at least three times. Results are presented in means ± SD. Statistical analyses were performed using Prism7 software (GraphPad Software). Tests for significance between groups were performed using an unpaired Student's t test or one-way ANOVA followed by a post hoc Tukey test. The significance threshold is $p < 0.05$.

Supplementary Material

Refer to Web version on PubMed Central for supplementary material.

Acknowledgments

We thank the zebrafish community for sharing reagents and Gaurav Ahuja for help with DiI injections. Work in M.H.'s laboratory was supported by the German Research Foundation (DFG, CECAD, GRK 1960) and the National Institute of General Medical Sciences (GM63904).

References

Biag J, Huang Y, Gou L, Hintiryan H, Askarinam A, Hahn JD, Toga AW, Dong HW. Cyto- and chemoarchitecture of the hypothalamic paraventricular nucleus in the C57BL/6J male mouse: a study of immunostaining and multiple fluorescent tract tracing. J Comp Neurol. 2012; 520:6–33. [PubMed: 21674499]

Cerdá-Reverter JM, Agulleiro MJ, R RG, Sánchez E, Ceinos R, Rotllant J. Fish melanocortin system. Eur J Pharmacol. 2011; 660:53–60. [PubMed: 21208603]

Chen Y, Lin YC, Kuo TW, Knight ZA. Sensory detection of food rapidly modulates arcuate feeding circuits. Cell. 2015; 160:829–841. [PubMed: 25703096]

Curado S, Stainier DY, Anderson RM. Nitroreductasemediated cell/tissue ablation in zebrafish: a spatially and temporally controlled ablation method with applications in developmental and regeneration studies. Nat Protoc. 2008; 3:948–954. [PubMed: 18536643]

Davison JM, Akitake CM, Goll MG, Rhee JM, Gosse N, Baier H, Halpern ME, Leach SD, Parsons MJ. Transactivation from Gal4-VP16 transgenic insertions for tissue-specific cell labeling and ablation in zebrafish. Dev Biol. 2007; 304:811–824. [PubMed: 17335798]

Dhillo WS, Small CJ, Seal LJ, Kim MS, Stanley SA, Murphy KG, Ghatei MA, Bloom SR. The hypothalamic melanocortin system stimulates the hypothalamo-pituitary-adrenal axis in vitro and in vivo in male rats. Neuroendocrinology. 2002; 75:209–216. [PubMed: 11979051]

Eigler T, Ben-Shlomo A. Somatostatin system: molecular mechanisms regulating anterior pituitary hormones. J Mol Endocrinol. 2014; 53:R1–R19. [PubMed: 24780840]

Enriori PJ, Evans AE, Sinnayah P, Jobst EE, Tonelli-Lemos L, Billes SK, Glavas MM, Grayson BE, Perello M, Nillni EA, et al. Diet-induced obesity causes severe but reversible leptin resistance in arcuate melanocortin neurons. Cell Metab. 2007; 5:181–194. [PubMed: 17339026]

Farooqi IS, Yeo GS, Keogh JM, Aminian S, Jebb SA, Butler G, Cheetham T, O'Rahilly S. Dominant and recessive inheritance of morbid obesity associated with melanocortin 4 receptor deficiency. J Clin Invest. 2000; 106:271–279. [PubMed: 10903343]

Forlano PM, Cone RD. Conserved neurochemical pathways involved in hypothalamic control of energy homeostasis. J Comp Neurol. 2007; 505:235–248. [PubMed: 17879270]

Friedman J. 20 years of leptin: leptin at 20: an overview. J Endocrinol. 2014; 223:T1–T8. [PubMed: 25121999]

Friedman J. The long road to leptin. J Clin Invest. 2016; 126:4727–4734. [PubMed: 27906690]

Garfield AS, Shah BP, Burgess CR, Li MM, Li C, Steger JS, Madara JC, Campbell JN, Kroeger D, Scammell TE, et al. Dynamic GABAergic afferent modulation of AgRP neurons. Nat Neurosci. 2016; 19:1628–1635. [PubMed: 27643429]

Gesta S, Tseng YH, Kahn CR. Developmental origin of fat: tracking obesity to its source. Cell. 2007; 131:242–256. [PubMed: 17956727]

Ghamari-Langroudi M, Srisai D, Cone RD. Multinodal regulation of the arcuate/paraventricular nucleus circuit by leptin. Proc Natl Acad Sci USA. 2011; 108:355–360. [PubMed: 21169216]

He Q, Karlberg J. Bmi in childhood and its association with height gain, timing of puberty, and final height. Pediatr Res. 2001; 49:244–251. [PubMed: 11158521]

Herget U, Wolf A, Wullimann MF, Ryu S. Molecular neuroanatomy and chemoarchitecture of the neurosecretory preoptic-hypothalamic area in zebrafish larvae. J Comp Neurol. 2014; 522:1542–1564. [PubMed: 24127437]

Hess ME, Hess S, Meyer KD, Verhagen LA, Koch L, Brönneke HS, Dietrich MO, Jordan SD, Saletore Y, Elemento O, et al. The fat mass and obesity associated gene (Fto) regulates activity of the dopaminergic midbrain circuitry. Nat Neurosci. 2013; 16:1042–1048. [PubMed: 23817550]

Huszar D, Lynch CA, Fairchild-Huntress V, Dunmore JH, Fang Q, Berkemeier LR, Gu W, Kesterson RA, Boston BA, Cone RD, et al. Targeted disruption of the melanocortin-4 receptor results in obesity in mice. Cell. 1997; 88:131–141. [PubMed: 9019399]

Imrie D, Sadler KC. White adipose tissue development in zebrafish is regulated by both developmental time and fish size. Dev Dyn. 2010; 239:3013–3023. [PubMed: 20925116]

Kim MS, Small CJ, Stanley SA, Morgan DG, Seal LJ, Kong WM, Edwards CM, Abusnana S, Sunter D, Ghatei MA, Bloom SR. The central melanocortin system affects the hypothalamo-pituitary thyroid axis and may mediate the effect of leptin. J Clin Invest. 2000; 105:1005–1011. [PubMed: 10749579]

King CM, Hentges ST. Relative number and distribution of murine hypothalamic proopiomelanocortin neurons innervating distinct target sites. PLoS ONE. 2011; 6:e25864. [PubMed: 21991375]

Kizil C, Brand M. Cerebroventricular microinjection (CVMI) into adult zebrafish brain is an efficient misexpression method for forebrain ventricular cells. PLoS ONE. 2011; 6:e27395. [PubMed: 22076157]

Krashes MJ, Lowell BB, Garfield AS. Melanocortin-4 receptor-regulated energy homeostasis. Nat Neurosci. 2016; 19:206–219. [PubMed: 26814590]

Krude H, Biebermann H, Schnabel D, Tansek MZ, Theunissen P, Mullis PE, Grüters A. Obesity due to proopiomelanocortin deficiency: three new cases and treatment trials with thyroid hormone and ACTH4-10. J Clin Endocrinol Metab. 2003; 88:4633–4640. [PubMed: 14557433]

Leibold S, Hammerschmidt M. Long-term hyperphagia and caloric restriction caused by low- or high-density husbandry have differential effects on zebrafish postembryonic development, somatic growth, fat accumulation and reproduction. PLoS ONE. 2015; 10:e0120776. [PubMed: 25799180]

Löhr H, Ryu S, Driever W. Zebrafish diencephalic A11-related dopaminergic neurons share a conserved transcriptional network with neuroendocrine cell lineages. Development. 2009; 136:1007–1017. [PubMed: 19234064]

Lu D, Willard D, Patel IR, Kadwell S, Overton L, Kost T, Luther M, Chen W, Woychik RP, Wilkison WO, et al. Agouti protein is an antagonist of the melanocyte-stimulating-hormone receptor. Nature. 1994; 371:799–802. [PubMed: 7935841]

Martin NM, Houston PA, Patterson M, Sajedi A, Carmignac DF, Ghatei MA, Bloom SR, Small CJ. Abnormalities of the somatotrophic axis in the obese agouti mouse. Int J Obes. 2006; 30:430–438.

Martinelli CE, Keogh JM, Greenfield JR, Henning E, van der Klaauw AA, Blackwood A, O'Rahilly S, Roelfsema F, Camacho-Hübner C, Pijl H, Farooqi IS. Obesity due to melanocortin 4 receptor (MC4R) deficiency is associated with increased linear growth and final height, fasting hyperinsulinemia, and incompletely suppressed growth hormone secretion. J Clin Endocrinol Metab. 2011; 96:E181–E188. [PubMed: 21047921]

McMenamin SK, Minchin JEN, Gordon TN, Rawls JF, Parichy DM. Dwarfism and increased adiposity in the gh1 mutant zebrafish vizzini. Endocrinology. 2013; 154:1476–1487. [PubMed: 23456361]

Myers MG Jr. Leptin keeps working, even in obesity. Cell Metab. 2015; 21:791–792. [PubMed: 26039442]

O'Rahilly S. 20 years of leptin: what we know and what the future holds. J Endocrinol. 2014; 223:E1–E3. [PubMed: 25143632]

Ottaway N, Mahbod P, Rivero B, Norman LA, Gertler A, D'Alessio DA, Perez-Tilve D. Diet-induced obese mice retain endogenous leptin action. Cell Metab. 2015; 21:877–882. [PubMed: 25980347]

Parichy DM, Elizondo MR, Mills MG, Gordon TN, Engeszer RE. Normal table of postembryonic zebrafish development: staging by externally visible anatomy of the living fish. Dev Dyn. 2009; 238:2975–3015. [PubMed: 19891001]

Peter RE. The preoptic nucleus in fishes: a comparative discussion of function-activity relationships. Am Zool. 1977; 17:775–785.

Randlett O, Wee CL, Naumann EA, Nnaemeka O, Schoppik D, Fitzgerald JE, Portugues R, Lacoste AM, Riegler C, Engert F, Schier AF. Whole-brain activity mapping onto a zebrafish brain atlas. Nat Methods. 2015; 12:1039–1046. [PubMed: 26778924]

Sabatier N, Caquineau C, Dayanithi G, Bull P, Douglas AJ, Guan XMM, Jiang M, Van der Ploeg L, Leng G. Alpha-melanocyte-stimulating hormone stimulates oxytocin release from the dendrites of hypothalamic neurons while inhibiting oxytocin release from their terminals in the neurohypophysis. J Neurosci. 2003; 23:10351–10358. [PubMed: 14614094]

Savastano S, Di Somma C, Barrea L, Colao A. The complex relationship between obesity and the somatropic axis: the long and winding road. Growth Horm IGF Res. 2014; 24:221–226. [PubMed: 25315226]

Song Y, Cone RD. Creation of a genetic model of obesity in a teleost. FASEB J. 2007; 21:2042–2049. [PubMed: 17341684]

Taniguchi H, He M, Wu P, Kim S, Paik R, Sugino K, Kvitsiani D, Fu Y, Lu J, Lin Y, et al. A resource of Cre driver lines for genetic targeting of GABAergic neurons in cerebral cortex. Neuron. 2011; 71:995–1013. [PubMed: 21943598]

Tauber M, Rochiccioli P. Exploration of the somatotropic axis. Diabetes Metab. 1996; 22:240–244. [PubMed: 8767169]

Timper K, Brüning JC. Hypothalamic circuits regulating appetite and energy homeostasis: pathways to obesity. Dis Model Mech. 2017; 10:679–689. [PubMed: 28592656]

Van Cauter E, Plat L, Copinschi G. Interrelations between sleep and the somatotropic axis. Sleep. 1998; 21:553–566. [PubMed: 9779515]

Varela L, Horvath TL. Leptin and insulin pathways in POMC and AgRP neurons that modulate energy balance and glucose homeostasis. EMBO Rep. 2012; 13:1079–1086. [PubMed: 23146889]

Vogt MC, Paeger L, Hess S, Steculorum SM, Awazawa M, Hampel B, Neupert S, Nicholls HT, Mauer J, Hausen AC, et al. Neonatal insulin action impairs hypothalamic neurocircuit formation in response to maternal high-fat feeding. Cell. 2014; 156:495–509. [PubMed: 24462248]

Wang D, He X, Zhao Z, Feng Q, Lin R, Sun Y, Ding T, Xu F, Luo M, Zhan C. Whole-brain mapping of the direct inputs and axonal projections of POMC and AgRP neurons. Front Neuroanat. 2015; 9:40. [PubMed: 25870542]

Yaswen L, Diehl N, Brennan MB, Hochgeschwender U. Obesity in the mouse model of pro-opiomelanocortin deficiency responds to peripheral melanocortin. Nat Med. 1999; 5:1066–1070. [PubMed: 10470087]

Zhang Y, Proenca R, Maffei M, Barone M, Leopold L, Friedman JM. Positional cloning of the mouse obese gene and its human homologue. Nature. 1994; 372:425–432. [PubMed: 7984236]

Zhang C, Forlano PM, Cone RD. AgRP and POMC neurons are hypophysiotropic and coordinately regulate multiple endocrine axes in a larval teleost. Cell Metab. 2012; 15:256–264. [PubMed: 22245570]

Highlights

- Sst neurons are second-order neurons of the central melanocortin system
- Pomc neurons stimulate Sst neurons, resulting in reduced growth hormone levels
- Excessive feeding leads to leptin resistance and decreased *pomc* expression
- Reduced *pomca* transcription favors somatic growth when food resources are plentiful

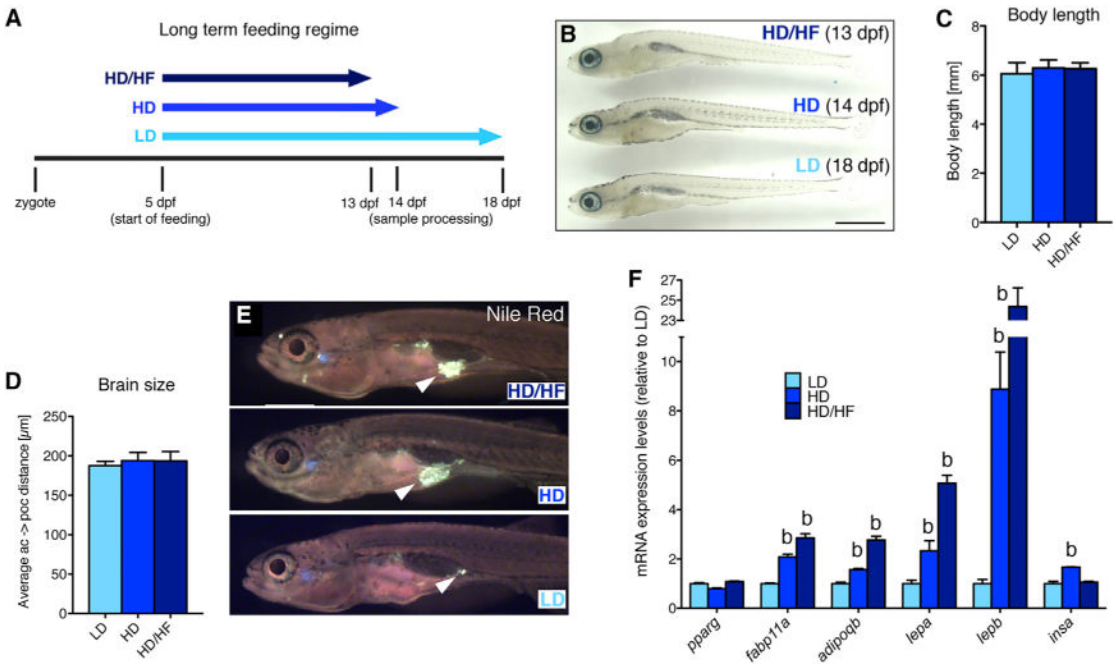

Figure 1. Effects of Long-Term Caloric Excess on Linear Growth and Lipid Metabolism in Larval Zebrafish

(A) Feeding paradigm for generation of size-matched zebrafish larvae with different caloric energy input (see text for details). Samples were collected at a standard body length of 6 mm at 13 dpf (HD/HF), 14 dpf (HD), and 18 dpf (LD).

(B) Lateral view of treated larvae.

(C and D) Quantification of body length (n = 20 for each group) (C) and distance between anterior and postoptic commissures as a measure for brain size (D) in *pomca:EGFPras* transgenic fish (see Figure 3; n = 10).

(E) Nile red staining of visceral lipids (arrowheads).

(F) qRT-PCR analyses of mRNA levels for *pparg*, *fabp11a*, *adipoqb*, *lepa*, *lepb*, and *insa*. Scale bar in (B) represents 1 mm. b, $p < 0.01$ relative to respective LD groups (F). Error bars in (C), (D), and (F) show SD.

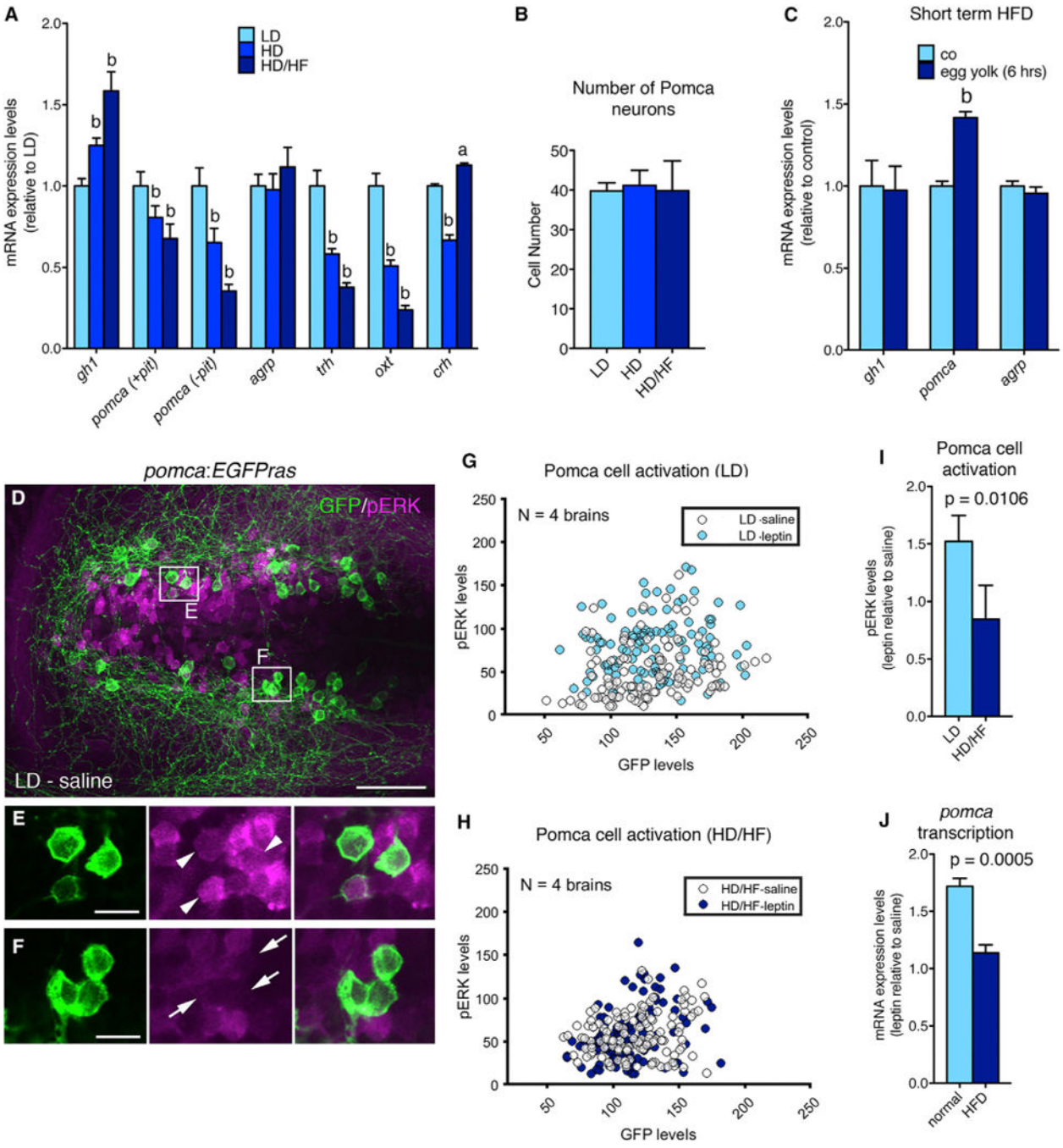

Figure 2. Long-Term Overfeeding Causes Leptin Resistance and Has an Impact on Both the Melanocortin and GH Systems

(A) qRT-PCR analyses of mRNA levels for *gh1*, *pomca*, *agrp*, *trh*, *oxt*, and *crh*. Corticotropin-releasing hormone (Dhillo et al., 2002) (*crh*) was downregulated in the HD group, but not in the HD/HF group, possibly pointing to stress responses caused by incubation in egg yolk medium. To specifically assess hypothalamic *pomca* expression levels, the pituitary was removed in *pomca* (−pit).

(B) Number of Pomca neurons in three feeding groups as determined by anti-GFP IF and cell counts in *pomca:EGFPras* fish (see Figure 3; n = 10).

(C) mRNA levels of *gh1*, *pomca*, and *agrp* after short-term application of egg yolk to 14 dpf larvae.

(D–F) IF for GFP and pERK on an exemplary *pomca:EGPras* transgenic larval brain (see Figure 3) subjected to the LD feeding regimen and incubated in saline.

(D) Overview of hypothalamic regions with GFP+/pERK+ domains.

(E and F) Magnification of areas boxed in (D) revealing GFP+/pERK+ cells (E, arrowheads) and GFP+/pERK-cells (F, arrows).

(G–I) pERK and GFP levels in Pomca neurons of size-matched LD (G) and HD/HF (H) *pomca:EGFPras* larvae treated for 30 min with saline or leptin (n = 4 for each condition), and quantification of normalized values (I).

(J) Relative *pomca* mRNA levels in juveniles subjected to normal feeding (n = 8) or high-fat diet (HFD; n = 7) for 10 days, 4 hr after ICV injection of recombinant leptin, determined via qRT-PCR normalized against saline-injected controls.

Scale bars represent 50 μm (D) and 10 μm (E and F). a, $p < 0.05$; b, $p < 0.01$ relative to respective LD groups (A and C). Error bars in (A)–(C), (I), and (J) show SD.

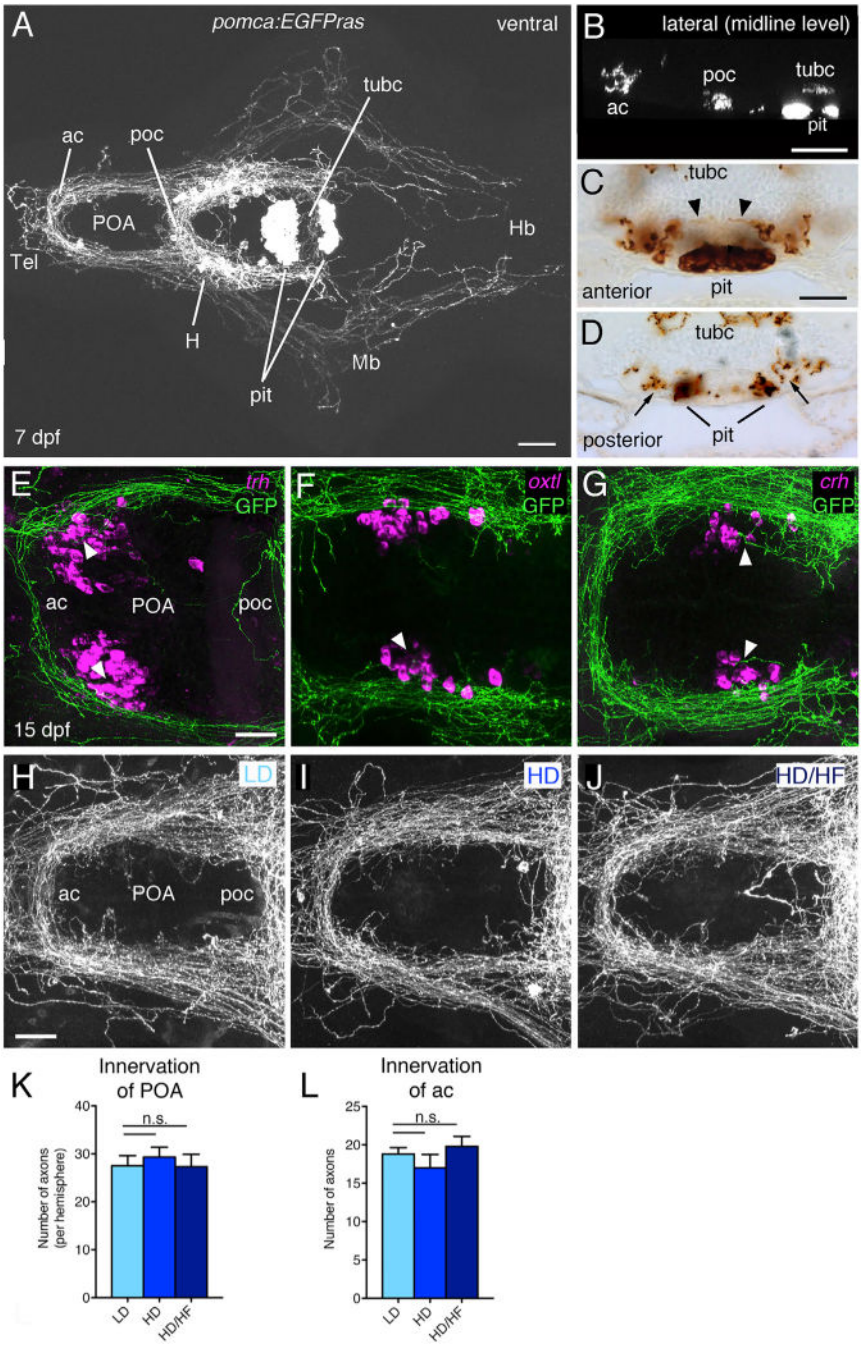

Figure 3. Analysis of Pomca Circuitry Reveals Sparse Pituitary Innervation by Pomca Axons and Unaltered POA Innervation after Excessive Feeding

(A–D) Anti-GFP IF (A and B) or immunohistochemistry (IHC) (C and D) on transgenic *pomca:EGFPras* larvae at 7 dpf.

(A) Cell bodies and projections of Pomca neurons in the hypothalamus (H) and *pomca+* pituicytes (pit) in the adenohypophysis are labeled. Pomca neurons project to telencephalon (Tel), preoptic area (POA), midbrain (Mb), and hindbrain (Hb).

(B) Optical sagittal section at the level of the midline depicting Pomca axons crossing the anterior (ac), postoptic (poc), and the posterior tuberculum commissure (tubc) dorsal to the pituitary.
(C and D) Cross sections at anterior (C) and posterior (D) levels of the pituitary; Pomca axons are dorsal (arrowheads; entering neurohypophysis) or lateral (arrows) of the Pomca pituicytes of the adenohypophysis (pit).
(E–G) Fluorescent *in situ* hybridization (ISH) for *trh* (E), *oxt* (F), and *crh* (G) neurons in the POA (arrowheads) combined with anti-GFP IF in *pomca:EGFPras* larvae at 15 dpf.
(H–L) Unaltered POA innervation in *pomca:EGFPras* larvae subjected to LD (H), HD (I), or HD/HF (J) treatments, revealed by anti-GFP IF and subsequent quantification of axon number in the POA (K; n = 5) or anterior commissure (ac; L; n = 5).
Scale bars represent 100 μm (A and B), 50 μm (C and D), and 25 μm (E–J); n.s., not significant. Error bars in (K) and (L) show SD.

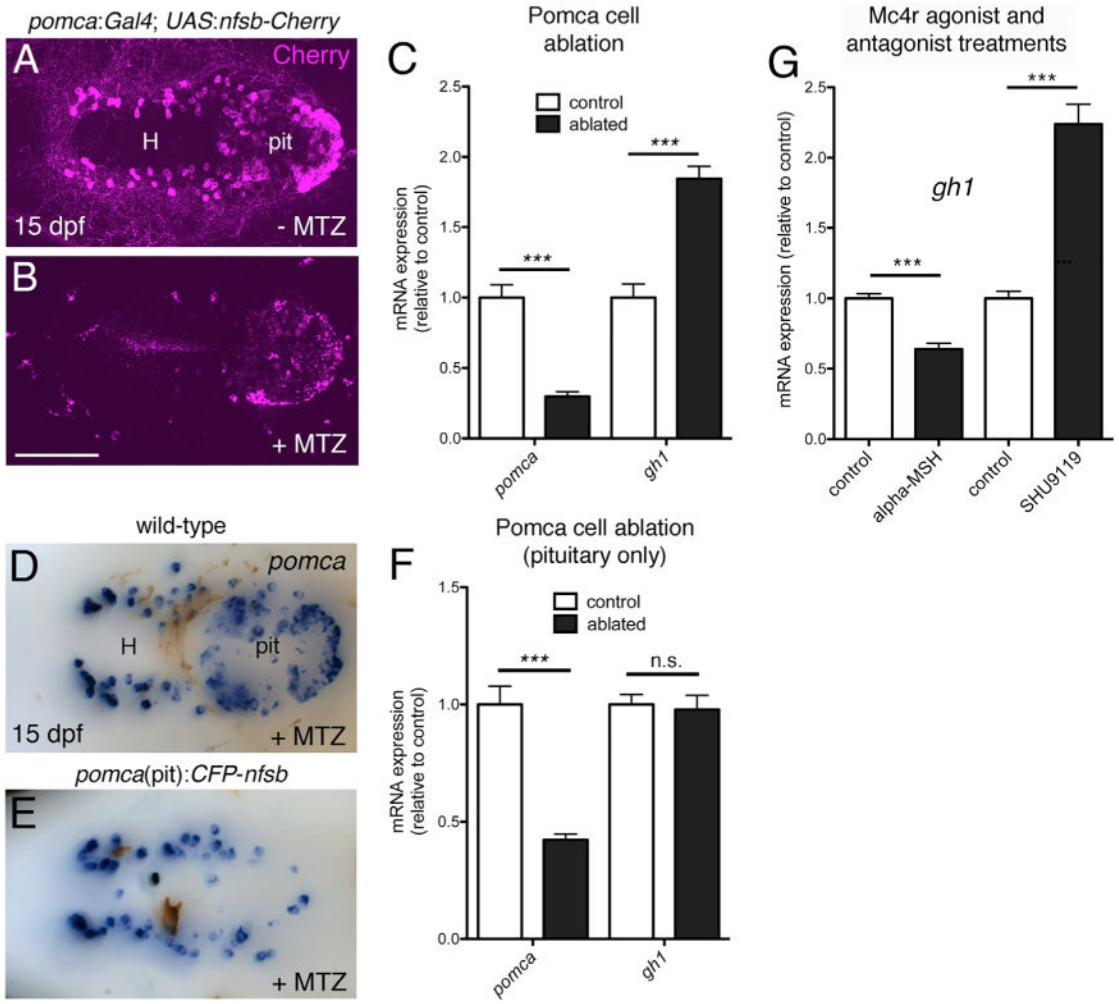

Figure 4. Pomca/αMSH Has a Negative Effect on *gh1* Expression

(A–C) Ablation of Pomca cells in hypothalamus and pituitary. Anti-RFP IF in *pomca:KalTA4*;*UAS:nfsb-Cherry* double transgenic larvae (15 dpf) without (A) or with MTZ treatment (B). (C) qRT-PCR analysis on *pomca:KalTA4* single transgenic larvae (control) compared to *pomca:KalTA4*;*UAS:nfsb-Cherry* double transgenic larvae (ablated) after 48-hr MTZ treatment revealing reduction of *pomca* (pointing to an ablation efficacy of ~75%) and elevation of *gh1* transcript levels.

(D–F) Pituitary specific ablation of Pomca cells. *pomca* ISH on MTZ-treated wild-type (D) and *pomca(pit):CFP-nfsb* transgenic (E) larvae at 15 dpf. (F) Selective loss of *pomca* in the pituitary results in decreased *pomca* levels but does not affect *gh1* expression as assessed by qRT-PCR. Abbreviations: pit, pituitary; H, hypothalamus.

(G) qRT-PCR analysis of *gh1* levels after treatment of 14 dpf zebrafish larvae with αMSH or SHU9119. Ventral views are shown in (A), (B), (D), and (E).

Scale bars represent 100 μm (A, B, D, and E); ***p < 0.001; n.s., not significant. Error bars in (C), (F), and (G) show SD.

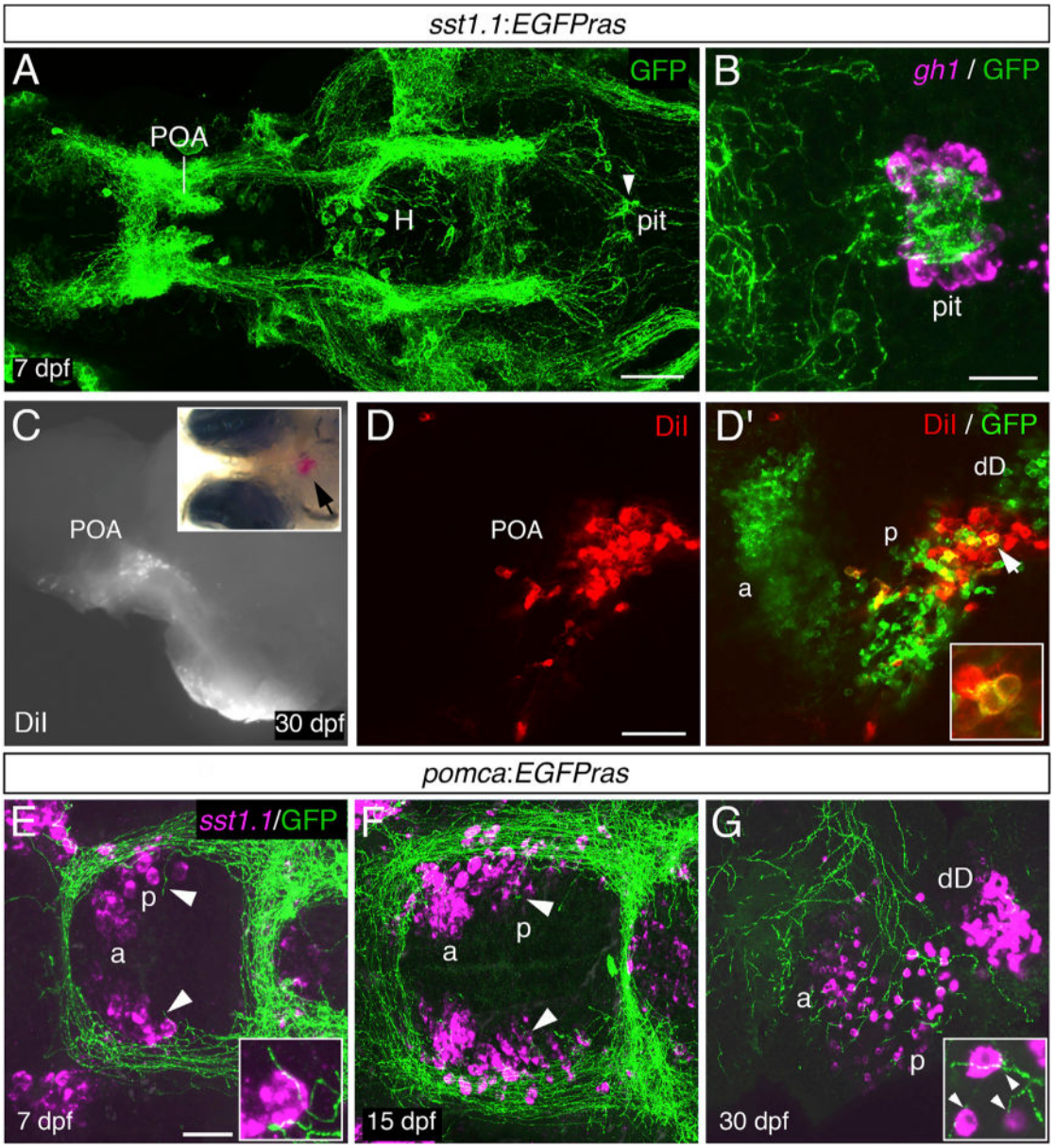

Figure 5. Sst1.1-Neurons of a Posterior POA Domain Project to Pituitary Somatotropes and Are Innervated by Pomca Cell Axons

(A) Anti-GFP IF on an *sst1.1:EGFPras* transgenic larva at 7 dpf. GFP+ axons innervating the pituitary (pit) are indicated by an arrowhead. H, hypothalamus; POA, preoptic area. (B) *gh1* ISH (magenta) co-stained via anti-GFP IF (green) at 7 dpf reveals extensive innervation of the *gh1* domain in the adenohypophysis by GFP+ Sst1.1 axons. (C–D′) Placement of DiI crystals into the pituitary of *sst1.1:EGFPras* fish at 30 dpf (C) retrogradely labels cell bodies in the POA (see arrowhead in inset for position of DiI). (D and D′) Within the POA, the posterior (p), but not the anterior (a) Sst1.1-cell domain, contains DiI+ cells. (D′, inset) Magnification of the region labeled by the arrowhead. Additional Sst1.1 cells (dD) are located outside the POA.

(E–G) *sst1.1* ISH combined with anti-GFP IF in *pomca:EGFPras* transgenic at 7 dpf (E), 15 dpf (F), and 30 dpf (G) showing innervation of the posterior Sst1.1 POA domain by Pomca-cell axons at all examined stages (see arrowheads and magnifications).
Scale bars represent 100 μm (A), 25 μm (B, E, and F), and 50 μm (D and G). Ventral views are shown in (A), (B), (E), and (F), and lateral views are shown in (C)–(D′) and (G).

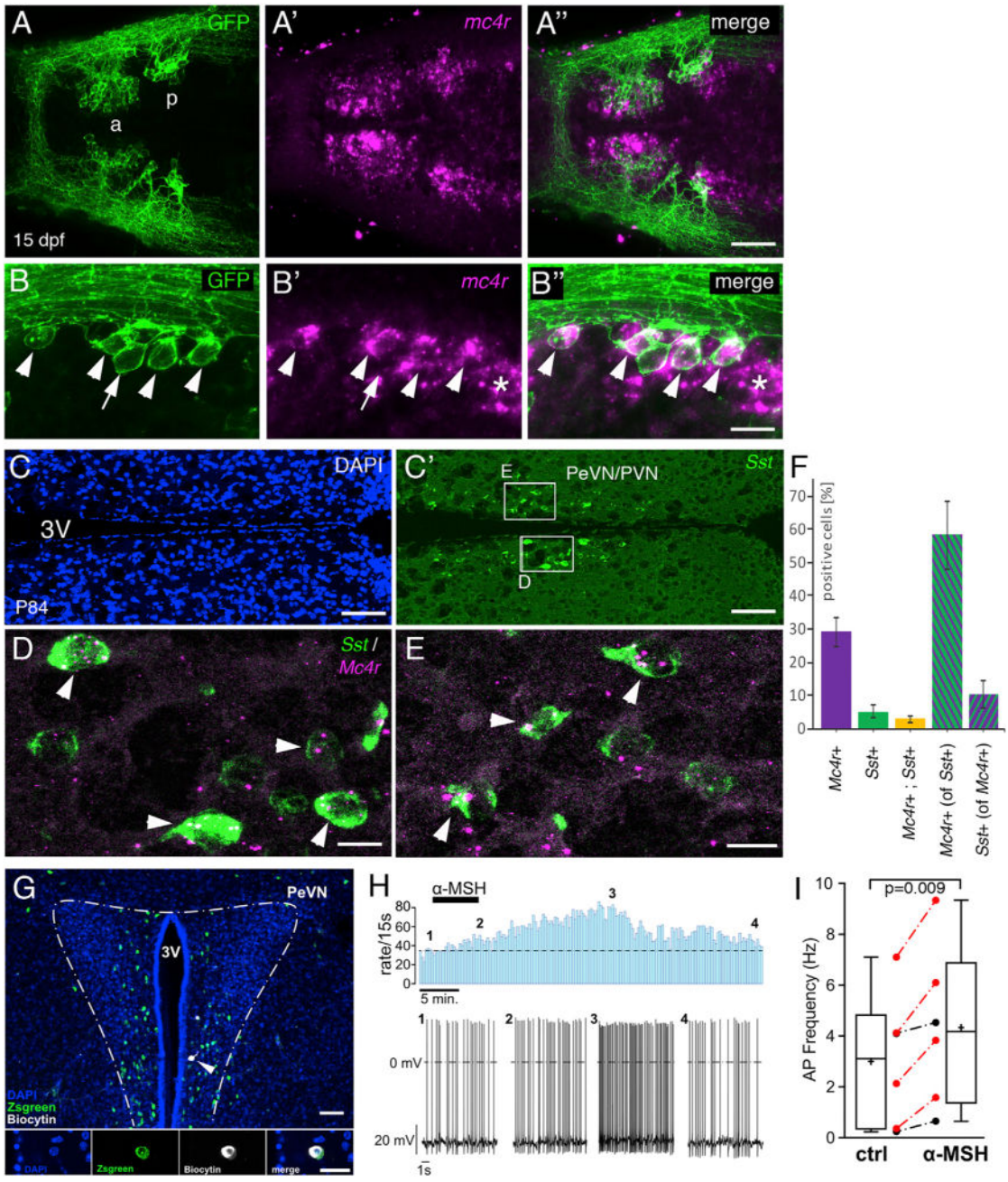

Figure 6. Hypophysiotropic Sst Neurons in Zebrafish and Mouse Express *mc4r* Transcript and Respond to αMSH in Mouse

(A–B″) *sst1.1:EGFPras* transgenic zebrafish at 15 dpf, stained via anti-GFP IF (green; [A] and [B]) in combination with *mc4r* ISH (magenta; [A′] and [B′]). Merged images are shown in (A″) and (B″).

(A–A″) Overview of the POA showing mc4r+ cells in Sst1.1+ neurons of anterior (a) and posterior (p) POA clusters.

(B–B″) Magnification of the posterior POA domain revealing expression of *mc4r* by most GFP+ cells (arrowheads, mc4r+, sst1+; arrow, mc4r−, sst1+; asterisk, mc4r+, sst1−).

(C–E) ISH for *Sst* (green; [C′]–[E]) and *Mc4r* (red; [D] and [E]) on sections of P84 mouse brains, counterstained with DAPI (nuclei, blue; [C]).
(C and C′) Overview of the PeVN/PVN hypothalamic region containing hypopyhsiotropic Sst cells.
(D and E) Magnification of boxed areas in (C′). Mc4r+ Sst neurons are marked by arrowheads.
(F) Quantification of Mc4r+ and Sst+ cells relative to total cell number (DAPI+), and quantification of Mc4r+ cells relative to Sst+ cells and vice versa (in percentage). Error bars show SD.
Scale bars represent 50 μm (A″), 25 μm (B″), 100 μm (C and C′), and 15 μm (D and E).
(G–I) αMSH increases the activity of Sst neurons in the PeVN of SstZsGreen mice.
(G) Top: overview of the PeVN (300 μm brain slice) showing ZsGreen immunofluorescence (green) and the Sst neuron that was labeled with biocytin (white, arrow) during the recording (blue, DAPI). Bottom: higher-magnified view of a single optical section of recorded neuron's soma showing the DAPI−, Sst−, and biocytin label separately and merged (from left to right). Scale bars: overview, 50 μm; details, 20 μm. αMSH modulation of single Sst PeVN neuron (H). Firing rates (bin width 15 s) before, during, and after application of 250 nM αMSH (indicated by bar) (top). Original traces from the recording at indicated time points 1–4 (bottom). Boxplots showing the effect of αMSH (250 nM, 5–7 min) on the action potential frequency of Sst neurons measured 10 min after onset of αMSH application ($p = 0.009$, $n = 6$, from 5 mice; paired two-tailed t test) (I). Red symbols indicate neurons in which the increase in action potential frequency was larger than 3 × SD of the control, thus defining them as responsive. Whiskers indicate the minimum and maximum, and plus signs and horizontal lines indicate means and medians, respectively; error bars indicate SD.

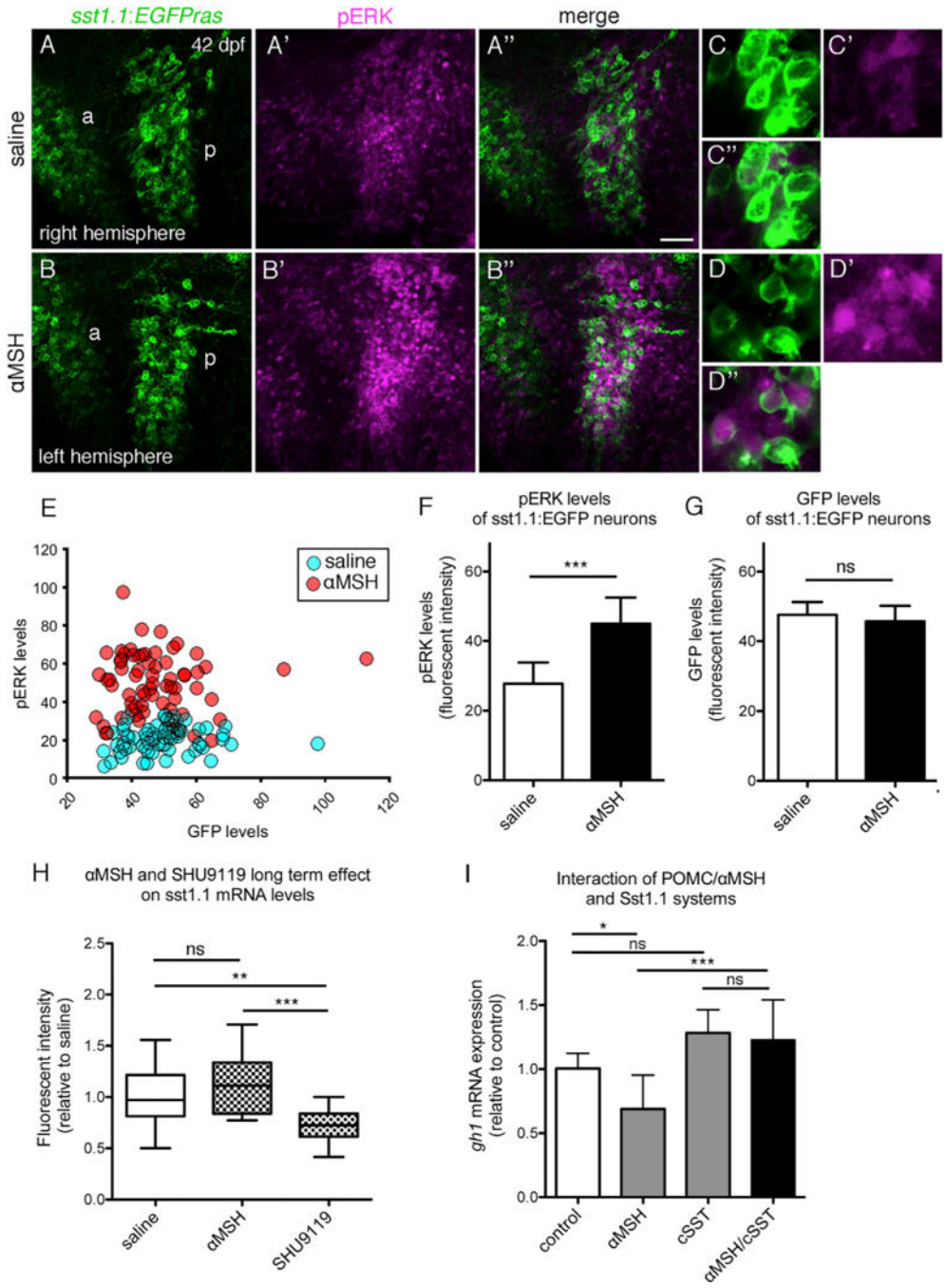

Figure 7. Zebrafish Sst Neurons Respond to αMSH to Mediate αMSH's Effect on GH Expression

(A–G) pERK response of hypophysiotropic Sst1.1 cells to αMSH treatment in *sst1.1:EGFPras* fish (42 dpf).

(A–B″) POA of two hemispheres derived from the same brain, differentially incubated in saline (A–A″) or 10 μM αMSH (B–B″) for 30 min. Double IF for GFP (green) and pERK (magenta) reveals increase in pERK levels after αMSH application in the posterior POA (p). Images of the right hemisphere were flipped horizontally.

(C–D″) Magnification of posterior POA Sst1.1 neurons without (C–C″) or with (D–D″) αMSH treatment.

(E–G) Quantification of pERK (E and F) and GFP (E and G) levels in a total of seven brain hemisphere pairs as shown in (A) and (B), revealing significantly increased pERK, but unaltered GFP levels in posterior Sst1.1 neurons after αMSH treatment.

(H) Effect of long-term αMSH or SHU9119 treatment on *sst1.1* mRNA levels. *sst1.1* FISH and signal intensity determination from confocal images of juvenile fish (42 dpf) that had been subjected to three repetitive ICV injections of αMSH, SHU9119, or saline over the course of 48 hr.

(I) Epistasis between Pomca/αMSH and Sst systems; *gh1* expression levels assessed by qRT-PCR analysis after treatment of larvae (14 dpf) for 8 hr with 10 μM αMSH, 1 μM cSST, or a combination of both peptides.

Scale bars represent 50 μm (A–B″) and 10 μm (C–D″). *$p < 0.05$; **$p < 0.01$; ***$p < 0.001$. Error bars in (F)–(I) show SD.